HHS Public Access

Author manuscript

AJNR Am J Neuroradiol. Author manuscript; available in PMC 2019 September 01.

Published in final edited form as:

AJNR Am J Neuroradiol. 2019 March ; 40(3): 510–516. doi:10.3174/ajnr.A5970.

Local Hemodynamic Conditions Associate with Focal Changes in the Intracranial Aneurysm Wall

Juan R. Cebral[1], **Felicitas Detmer**[1], **Bong Jae Chung**[1], **Joham Choque-Velasquez**[2], **Behnam Rezai**[2], **Hanna Lehto**[2], **Riikka Tulamo**[2,3], **Juha Hernesniemi**[2], **Mika Niemela**[2], **Alexander Yu**[4], **Richard Williamson**[4], **Khaled Aziz**[4], **Sophia Sakur**[5], **Sepideh Amin-Hanjani**[5], **Fady Charbel**[5], **Yasutaka Tobe**[6], **Anne Robertson**[6], and **Juhana Frosen**[7]

[1]Bioengineering Department, Volgenau School of Engineering, George Mason University, Fairfax, Virginia, USA [2]Neurosurgery Research Group, Biomedicum Helsinki and Helsinki University Central Hospital, Helsinki, Finland [3]Department of Vascular Surgery, Helsinki University Central Hospital, Helsinki, Finland [4]Department of Neurosurgery Allegheny General Hospital, Pittsburgh, Pennsylvania, USA [5]Department of Neurosurgery, University of Illinois at Chicago, Chicago, Illinois, USA [6]Mechanical Engineering and Materials Science and Department of Bioengineering, Swanson School of Engineering, University of Pittsburgh, Pittsburgh, Pennsylvania, USA [7]Hemorrhagic Brain Pathology Research Group, Neurocenter, Kuopio University Hospital, Kuopio, Finland

Abstract

Background and Purpose: Aneurysm hemodynamics has been associated with wall histology and inflammation. We now investigated associations between local hemodynamics and focal wall changes visible intra-operatively.

Methods: Computational fluid dynamics models were constructed from 3D images of 65 aneurysms treated surgically. Aneurysm regions with different visual appearances were identified in intra-operative videos: 1) “atherosclerotic” (yellow), 2) “hyperplastic” (white), 3) “thin” (red), 4) rupture site, and 5) “normal” (similar to parent artery) and marked on 3D reconstructions. Regional hemodynamics was characterized by: wall shear stress (WSS), oscillatory shear index (OSI), relative residence time (RRT), WSS gradient and divergence, gradient oscillatory number (GON), and dynamic pressure (PRE); and compared with the Mann-Whitney test.

Results: Hyperplastic regions had lower average WSS ($p=0.005$) and pressure ($p=0.009$) than normal regions. Flow conditions in atherosclerotic and hyperplastic regions were similar, but had higher average RRT ($p=0.03$), and OSI ($p=0.04$) than thin regions. Hyperplastic regions also had higher average GON ($p=0.002$) than thin regions. Thin regions had lower average RRT ($p<0.001$), OSI ($p=0.006$), and GON ($p<0.001$) than normal regions, and higher average WSS ($p=0.006$) and pressure ($p=0.009$) than hyperplastic regions. Thin regions tended to be aligned with the flow stream, while atherosclerotic and hyperplastic regions with recirculation zones.

Corresponding Author: Juan R. Cebral, PhD, Bioengineering and Mechanical Engineering Departments, Volgenau School of Engineering, George Mason University, 4400 University Drive, MSN 2A1, Fairfax, VA 22030, USA, Phone: 703-993-4078, jcebral@gmu.edu.

Conclusions: Local hemodynamics is associated with visible focal wall changes. Slow swirling flow with low and oscillatory WSS associate with “atherosclerotic” and “hyperplastic” changes. High flow conditions prevalent in regions near the flow impingement site characterized by higher and less oscillatory WSS associate with local “thinning” of the wall.

Introduction

Unruptured intracranial aneurysms (UIA) are relatively frequent in the past middle age population, with a prevalence of approx. 3%[1]. Although most UIAs are asymptomatic and found incidentally, when diagnosed they cause significant concern because some may eventually rupture causing aneurysmal subarachnoid hemorrhage (aSAH) which has a mortality of approximately 40%[2]. Due to this sinister outcome of aSAH, many diagnosed UIAs are treated to prevent rupture. The currently available treatment options are, however, all invasive interventions that carry a significant risk of morbidity (5-7%) and even a low risk of mortality (1%)[3,4]. Interventions to prevent UIA rupture should therefore be focused to those UIAs that are indeed at risk of rupture, especially since many UIAs remain unruptured during the whole lifetime of their carrier[5].

Aneurysms rupture when the mechanical load imposed on their wall exceed the strength of the wall. This mechanical load may vary depending on physical activity, and hence the most important factor to consider when determining the risk of aneurysm rupture, is the strength of the aneurysm wall which can vary substantially across even UIAs[6]. Histological studies have shown that UIAs can have very different wall structure[7,8], which often is clear also in surgery when the UIA is exposed[9]. At the moment there are no diagnostic tools available to determine the structure of an UIA without direct visualization at surgery.

Flow interacts with the vessel wall and activates signaling pathways that regulate vessel wall remodeling[10]. Flows within aneurysms are not physiological and are influenced by the aneurysm and parent artery geometry, the position of the orifice on the parent artery, the local angio-architecture, among other factors[11]. However, flow conditions are statistically different between UIAs and ruptured IAs (RIAs)[12–14]. Recently we have shown an association between flow conditions and the overall wall histology of the intracranial aneurysm (IA), as well as with the degree of inflammatory cell infiltration in the IA wall[15]. Since our prior results suggest that global flow inside the IA fundus regulates the remodeling of the IA wall, we now investigated whether local flow conditions associate with the focal variations in IA wall structure observed at surgery.

Methods

Patients and Data

A total of 66 patients with intracranial aneurysms treated with surgical clipping were studied. Patients gave informed consent and the study was approved by the Institutional Review Boards of Helsinki University Hospital, Allegheny General Hospital and University of Illinois Chicago. Video recordings obtained during the surgical procedures were collected. Only aneurysms that were visibly exposed in the videos were included in the study. In the videos of 8 patients the aneurysm surface could not be reliably visualized and

these cases were discarded. One further case was excluded as it was observed to be heavily thrombosed. The remaining 57 patients harbored 65 aneurysms that were further studied. Prior to surgery, 37 patients of these patients were imaged with 3D computed tomography angiography (CTA) and 20 with 3D rotational angiography (3DRA). The aneurysm and patient characteristics are summarized in Supplementary Table I.

Hemodynamics Modeling

Computational fluid dynamics (CFD) models were constructed from the pre-surgical 3D images using previously described techniques[16]. Blood was mathematically modeled as an incompressible Newtonian fluid and the 3D unsteady Navier-Stokes equations were numerically solved using finite elements with an in-house software[17]. Pulsatile inflow boundary conditions were prescribed using flow waveforms measured in normal subjects and scaled with a power law of the area of the inflow vessel[18]. Outflow boundary conditions consistent with Murray's law were prescribed at the outlets[19]. Wall compliance was neglected, and no-slip boundary conditions were prescribed at the walls. Numerical simulations were run for two cardiac cycles using a timestep of 0.01 sec, and data from the second cycle were saved for analysis. From the results of the second cycle, the following quantities were computed at the aneurysm wall: oscillatory shear index (OSI), mean wall shear stress (WSS), mean wall shear stress divergence (WSSDIV), mean wall shear stress gradient (WSSGRD), mean gradient oscillatory number (GON), mean pressure (PRE), and relative residence time (RRT). Here, mean refers to the time average of these quantities over the cardiac cycle. The mathematical definitions of these quantities and their meanings are listed in Supplementary Table II.

Regional Analysis

Five types of aneurysm wall regions were considered according to their visual appearance in the surgical videos: 1) "atherosclerotic" (A) walls characterized by a yellow appearance, 2) "hyperplastic" (H) walls that appear as white, 3) "thin" (T) walls with a red translucent appearance, 4) rupture (R) site – visible as a hole in the wall or a hematoma attached to the rupture site (more details in Supplementary Figure I), and 5) "normal" (N) - the remainder of the wall which had no remarkable features. Note that the exact connection between the visual appearance and the histological characteristics of these regions remain to be established. Using a recently developed 3D virtual marking tool (ChePen3D)[20], the patient specific vascular geometry was rotated to the same orientation as the surgical view in a superposed a semi-transparent video frame where the aneurysm is exposed. The different wall regions visible in the video were then marked directly onto the CFD model with different color labels, enabling direct analysis of the relationship between flow and wall features. On average the area of the aneurysm not visible in the videos were 28.9% (±25.6%) of the total aneurysm area. Subsequent analysis was restricted to the visible regions. The marking was performed blinded to hemodynamic results. Examples of aneurysm markings are presented in Figure 1.

Once the aneurysm regions were labeled, the maximum (max), minimum (min) and average (avg) of each hemodynamic variable, normalized with the mean value over the aneurysm sac, was computed for each simply connected region of a given wall type. Subsequently, the

median and lower and upper quartiles of each variable over the five different wall types were computed, and the medians were statistically compared with the non-parametric Mann-Whitney U test. Pairwise differences were considered significant if $p<0.05$, and the p-values were adjusted for multiple testing.

Next, three multivariate statistical models were constructed using a regularized logistic regression (Lasso) approach, which reduces overfitting errors. The regularization parameters were computed using a 10-fold cross-validation strategy. In the first model, the atherosclerotic and hyperplastic regions were combined into a single group, and compared to the group of normal looking walls. In the second model, the thin regions were compared to the normal looking walls, and in the third model the atherosclerotic and hyperplastic regions combined were compared to the thin regions.

Finally, the location of the different wall regions were visually compared to global flow features such as the inflow jet, regions of flow recirculation and swirling flow, etc.

Results

The median and lower and upper quartiles of each hemodynamic variable over each of the five wall regions as well as the entire aneurysm sac are presented in Supplementary Table III. The p-values of pairwise comparisons between the pathological and normal looking wall regions are listed in Table 1, and between the different pathological wall regions in Table 2. For these comparisons, the hemodynamic variables were normalized with their values over the entire aneurysm sac, in order to facilitate the comparisons of regions from different aneurysms at different locations. Statistically significant differences adjusted for multiple regions testing are indicated with a “*”, and the region with the higher median is indicated in parenthesis. Variables that remain significant after further adjusting for multiple variable testing are indicated with a “**”.

Focal wall changes are associated with local flow conditions

Heterogeneous wall was observed in 59/65 (91%) of the studied lAs at surgery. When compared to wall regions that did not appear as hyperplastic, atherosclerotic, or thin during surgical exposure, the local flow conditions at the regions of remodeled wall were different (Supplementary Table IV). In general, normal looking walls had larger ranges (higher maximum and lower minimum) for all hemodynamic variables compared to pathological regions (either atherosclerotic, or hyperplastic, or thin, or ruptured).

Characteristics of flow in hyperplastic (white) and atherosclerotic (yellow) regions

Compared to normal looking regions, hyperplastic regions had lower mean wall shear stress (WSSavg, p=0.005) and mean pressure (PREavg, p=0.009). Mean variables were not significantly different between atherosclerotic and normal looking regions, except mean wall shear stress which was lower (WSSavg, p=0.01). Atherosclerotic and hyperplastic regions (Table 2) had statistically similar flow features, only minimum pressure was higher in the atherosclerotic regions (PREmin, p=0.01). Additionally, atherosclerotic and hyperplastic regions had statistically similar flow features to rupture regions except that the mean pressure was higher in the ruptured regions (PREavg, atherosclerotic vs. rupture: p=0.01;

hyperplastic vs. rupture: p=0.009). In contrast, compared to thin regions, atherosclerotic and hyperplastic regions had slower flows (higher RRTavg, atherosclerotic vs. thin: p=0.03; hyperplastic vs. thin: p<0.001), more oscillatory wall shear stress (OSIavg, atherosclerotic vs. thin: p=0.05; hyperplastic vs. thin: p=0.04) and more oscillatory shear stress gradients (hyperplastic vs. thin: GONavg, p=0.002).

Characteristics of flow in thin (red) regions

Compared to normal looking regions, thin (red) regions had faster flows (RRTavg, p<0.001), less oscillatory wall shear stress (OSIavg, p=0.006), and less oscillatory shear stress gradient (GONavg, p<0.001). Additionally, thin regions had higher wall shear stress (WSSavg) than hyperplastic (p=0.006) and rupture regions (p=0.01), and they had higher pressure than hyperplastic regions (PREavg, p=0.009) but not when compared to ruptured regions (p=0.09). Compared to rupture regions, thin regions also had larger wall shear stress (WSSavg, p=0.01).

Characteristics of flow at the sites of rupture

Compared to normal regions, the rupture sites had lower wall shear stress (WSSavg, p=0.005) and higher pressure (PREavg, p=0.03). Interestingly, the pressure (PREavg) was higher in rupture regions compared to atherosclerotic (p=0.01) and hyperplastic (p=0.009) regions, but lower than in thin regions (p=0.009).

Qualitative flow characteristics and wall appearance

Qualitatively, thin wall regions tend to be aligned with the flow stream in the aneurysm (approximately 86% of thin regions are aligned with the inflow jet). Thus, they tend to be in regions of faster flow that have higher wall shear stress (approximately 90% of thin regions are observed in regions of high or moderate WSS) and pressure (closer to flow impingement). In contrast, thick (atherosclerotic and hyperplastic) regions tend to be aligned with the ends of the intrasaccular vortices (approximately 61% of thick regions) which are normal to the flow stream. Thus, thick regions tend to coincide with locations of slow swirling flow (approximately 78% of these regions) that have low wall shear stress (approximately 85% of thick regions are observed in regions of low WSS), high residence time, and higher oscillatory wall shear stress and shear stress gradients.

An example is presented in Figure 2. In this case the aneurysm has a thin (red) region aligned with the inflow jet and under higher wall shear stress, and a hyperplastic (white) region under lower wall shear stress and that coincides with the end of a vortex core-line around which the flow swirls within the aneurysm. Further examples of aneurysms are presented in Supplementary Figures II-V.

Discrimination of aneurysm wall characteristics based on local flow conditions

Results of multivariate statistical models built to discriminate between the different aneurysm wall regions are presented in Supplementary Figure VI. This figure shows receiver operating characteristic (ROC) curves and calibration plots for the three models considered: a) atherosclerotic and hyperplastic vs. normal regions, b) thin vs. normal regions, and c) atherosclerotic and hyperplastic vs. thin regions. The corresponding areas under the curve

(AUC) were 0.92, 0.97 and 0.70, respectively. These AUC's indicate very good discrimination between the pathological and normal regions, and relatively good discrimination between thin and thickened wall regions. Visually, the calibration plots show reasonable fits to the data, with small deviations of the fitted lines from the 45° straight line which corresponds to a perfect goodness of fit.

The coefficients of each hemodynamic variable in each of the three models ordered by their importance (influence on the outcome and frequency of inclusion in the model during cross-validation) are presented in Supplementary Tables IV-VI. The most important variables to discriminate atherosclerotic and hyperplastic regions from normal regions were GON(min), RRT(avg), WSSGRAD(max), and OSI(min,avg). The most important variables to discriminate between thin and normal regions were WSSGRD(min,max), GON(avg), RRT(min,max) and PRE(max). Finally, the most important variables to discriminate atherosclerotic and hyperplastic from thin regions were RRT(avg,max), GON(max) and WSS(min).

Discussion

Flow and wall remodeling

The flow characteristics prevalent in "atherosclerotic" and "hyperplastic" thick regions of the aneurysm wall, are similar to those previously associated with atherosclerosis in arteries[21,22], namely low and oscillatory wall shear stress in regions of slow and recirculating flow. In the IAs these regions tend to be located near the end of intra-saccular vortex core-lines and towards the sides of the intra-aneurysmal flow stream. These observations suggest that such low flow conditions promote wall remodeling that results in local thickening of the wall. This conjecture needs to be further investigated to prove that indeed atherosclerotic (yellow) and hyperplastic (white) regions are thicker than normal looking walls as suggested by previous studies[23,24], and that their histological characteristics include lipid accumulation, cell proliferation, etc. Furthermore, although these regions may be thicker, this does not automatically imply that they are mechanically stronger. On the contrary, it is plausible that the wall structure and in particular the collagen fiber reinforcements in these regions are degraded resulting in an overall weaker wall region.

In contrast to "atherosclerotic" and "hyperplastic" regions, "thin" wall regions tend to be aligned with the flow stream and located towards the region where the inflow jet impacts the aneurysm wall. These results agree with previous studies where the authors reported the correlation between thin-region and impingement flow[25]. The local flow conditions in these regions seem similar to those that predispose arteries for aneurysm formation[14], i.e. faster flow and less oscillatory and higher wall shear stress and shear stress gradient. Another study of unruptured aneurysm walls found de-endothelialization as consistent feature in thinned regions[23]. Perhaps these are indications of impaired remodeling of these regions since the time of the aneurysm inception, or of degenerative remodeling associated with abnormally high flow conditions.

Flow as a trigger of aneurysm rupture

Rupture sites share some characteristics with “thin” wall regions and other characteristics with “atherosclerotic” and “hyperplastic” wall regions. Similarly to thin regions, they tend to be aligned with the inflow and have higher pressure (an indication of proximity to the flow impingement site) than thick wall regions. This is consistent with previous work where thin wall regions of unruptured aneurysms coincided with diverging WSS vector and a local rise in the pressure, again as an indicator of flow impingement[23–26]. An earlier study of pathological changes in the aneurysm wall found that thin hypocellular, de-endothelialized walls were always ruptured[27]. On the other hand, similarly to atherosclerotic and hyperplastic regions, rupture regions tend to have lower wall shear stress, higher oscillatory shear index and higher oscillations of the shear stress gradient than thin regions. These similarities and differences may suggest that there could be more than one failure mode of the aneurysm wall, one associated with thickened walls and another associated to thinned walls and are a subject of ongoing investigation.

Diagnostic application of computational fluid dynamics?

Local hemodynamic-based statistical models seem capable of discriminating between normal looking regions of the wall and regions of wall thinning or atherosclerotic thickening. On the one hand, this suggests that local flow conditions have an important influence on the local evolution and remodeling of the aneurysm wall, and on the other hand, that in principle they could be used as a surrogate biomarker of the wall status when evaluating patients with cerebral aneurysms.

Comparison to Previous Studies and Limitations

Several previous studies have investigated the relationship between hemodynamics and wall characteristics observed during surgery[9,28–33]. Comparisons with our findings are presented in Supplementary Table VII. In all the three studies that compared the hemodynamics at the site of rupture and elsewhere in the IA fundus, low WSS was characteristic to the site of rupture. Similarly, higher pressure was characteristic to thin regions in all the three studies investigating that, and prolonged relative residence time was characteristic to hyperplastic or atherosclerotic wall in all the four studies investigating thick or atherosclerotic walls. The observation that there are hemodynamic variables that consistently associate with IA wall characteristics in different studies despite slightly different methodology, study design, and different patient population, implies that these associations are real and potentially causal. Whether the other hemodynamic variables reported to associate with IA wall type in some of the studies without being replicated by others, are in fact associated with IA wall remodeling or perhaps just co-variates or co-incidental findings, remains to be determined by large studies with sufficient statistical power. These large studies comparing the flow dynamics and the characteristics of the IA wall are also needed to replicate our finding that IA wall type can be relatively accurately predicted with computational fluid dynamic models.

This study has several limitations. Arterial walls were approximated as rigid and blood as a Newtonian fluid. Patient-specific flow conditions were not available, and therefore typical flows from normal subjects were used. Flow variables were normalized with the average values over the aneurysm sac to compare the local hemodynamics of the different regions of

aneurysms at different locations. In general normalized values are more robust with respect to uncertainties in the inflow conditions. Minimum and maximum values of hemodynamic variables computed over tissue regions are less robust than mean values and require finer meshes for a more precise calculation. The identification of the different wall regions was performed subjectively by visual inspection of the intra-operative videos and marking the corresponding 3D models. Inaccuracies in the definition of small regions in places where the hemodynamic variables are highly heterogeneous can have an effect on the values computed over these regions. The reproducibility of region delineation was not assessed as the regions of each aneurysms were marked by one observer. Additionally, the assumptions that yellow regions correspond to atherosclerotic changes, white regions to hyperplastic changes, and red regions to thin de-cellularized regions need to be further demonstrated. Finally, the sample size limited the significance of some comparisons, such as those involving rupture sites (n=13). The trends identified in this study should be confirmed with larger samples.

Conclusions

Local flow conditions are associated to local remodeling of the aneurysm wall. Low flow conditions prevalent in regions of slow swirling flow characterized by low and oscillatory shear stress associate with “atherosclerotic” and “hyperplastic” changes of the wall. High flow conditions prevalent in regions near the flow impingement site characterized by higher and less oscillatory wall shear stress associate with local “thinning” of the wall. Local hemodynamics could in principle be used to identify local regions of the wall with different histological and structural properties. This study demonstrates the value of intra-operative data for understanding the role of intra-saccular hemodynamics in IA wall changes.

Supplementary Material

Refer to Web version on PubMed Central for supplementary material.

Acknowledgments

Funding

This work was supported by NIH grant #R01NS097457, and Kuopio University Hospital and Helsinki University Hospital research funds, and by a research grant from the Finnish Medical Foundation.

References

1. Vlak MH, Algra A, Brandenburg R, et al. Prevalence of unruptured intracranial aneurysms, with emphasis on sex, age, comorbidity, country, and time period: a systematic review and meta-analysis. Lancet Neurol 2011;10:626–36. [PubMed: 21641282]
2. Nieuwkamp DJ, Setz LE, Algra A, et al. Changes in case fatality of aneurysmal subarachnoid haemorrhage over time, according to age, sex, and region: a meta-analysis. Lancet Neurol 2009;8:635–42. [PubMed: 19501022]
3. Kotowski M, Naggara O, Darsaut TE, et al. Safety and occlusion rates of surgical treatment of unruptured intracranial aneurysms: a systematic review and meta-analysis of the literature from 1990 to 2011. J Neurol Neurosurg Psychiatry 2013;84:42–8. [PubMed: 23012447]
4. Naggara ON, White PM, Guilbert F, et al. Endovascular treatment of intracranial unruptured aneurysms: systematic review and meta-analysis of the literature on safety and efficacy. Radiology 2010;256:887–97. [PubMed: 20634431]

5. Korja M, Lehto H, Juvela S. Lifelong rupture risk of intracranial aneurysms depends on risk factors: a prospective Finnish cohort study. Stroke 2014;45:1958–63. [PubMed: 24851875]
6. Robertson AM, Duan X, Hill MR, et al. Diversity in the strength and structure of unruptured cerebral aneurysms. Ann Biomed Eng 2014;43:1502–15.
7. Kataoka K, Taneda M, Asai T, et al. Structural fragility and inflammatory response of ruptured cerebral aneurysms - A comparative study between ruptured and unruptured cerebral aneurysms. Stroke 1999;30:1396–401. [PubMed: 10390313]
8. Frosen J, Tulamo R, Paetau A, et al. Saccular intracranial aneurysm: pathology and mechanisms. Acta Neuropathol 2012;123:773–86. [PubMed: 22249619]
9. Kadasi LM, Dent WC, Malek AM. Colocalization of thin-walled dome regions with low hemodynamic wall shear stress in unruptured cerebral aneurysms. J Neurosurg 2013;119:172–9. [PubMed: 23540271]
10. Meng H, Tutino VM, Xiang J, et al. High WSS or Low WSS? Complex Interactions of Hemodynamics with Intracranial Aneurysm Initiation, Growth, and Rupture: Toward a Unifying Hypothesis. AJNR Am J Neuroradiol 10.3174/ajnr.A3558.
11. Sforza DM, Putman CM, Cebral JR. Hemodynamics of cerebral aneurysms. Annu Rev Fluid Mech 2009;41:91–107. [PubMed: 19784385]
12. Xiang J, Natarajan SK, Tremmel M, et al. Hemodynamic-morphologic discriminants for intracranial aneurysm rupture. Stroke 2011;42:144–52. [PubMed: 21106956]
13. Cebral JR, Mut F, Weir J, et al. Quantitative characterization of the hemodynamic environment in ruptured and unruptured brain aneurysms. AJNR Am J Neuroradiol 2011;32:145–51. [PubMed: 21127144]
14. Can A, Du R. Association of Hemodynamic Factors With Intracranial Aneurysm Formation and Rupture: Systematic Review and Meta-analysis. Neurosurgery 2016;78:510–20. [PubMed: 26516819]
15. Cebral J, Ollikainen E, Chung BJ, et al. Flow conditions in the intracranial aneurysm lumen are associated with inflammation and degenerative changes of the aneurysm wall. AJNR Am J Neuroradiol 2017;38:119–26. [PubMed: 27686488]
16. Cebral JR, Castro MA, Appanaboyina S, et al. Efficient pipeline for image-based patient-specific analysis of cerebral aneurysm hemodynamics: Technique and sensitivity. IEEE Trans Med Imag 2005;24:457–67.
17. Mut F, Aubry R, Löhner R, et al. Fast numerical solutions of patient-specific blood flows in 3D arterial systems. Int J Num Meth Biomed Eng 2010;26:73–85.
18. Cebral JR, Castro MA, Putman CM, et al. Flow-area relationship in internal carotid and vertebral arteries. Physiol Meas 2008;29:585–94. [PubMed: 18460763]
19. Painter PR, Eden P, Bengtsson HU. Pulsatile blood flow, shear force, energy dissipation and Murray's Law. Theor Biol Med Model 2006;3:31. [PubMed: 16923189]
20. Cebral JR, Mut F, Gade P, et al. Combining Data from Multiple Sources to Study Mechanisms of Aneurysm Disease: Tools and Techniques. Int J Numer Methods Biomed Eng 10.1002/cnm.3133.
21. Taylor CA, Hughes TJ, Zarins CK. Finite element modeling of three-dimensional pulsatile flow in the abdominal aorta: relevance to atherosclerosis. Ann Biomed Eng 1998;26:975–87. [PubMed: 9846936]
22. Peiffer V, Sherwin SJ, Weinberg PD. Does low and oscillatory wall shear stress correlate spatially with early atherosclerosis? A systematic review. Cardiovasc Res 2013;99:242–50. [PubMed: 23459102]
23. Tobe Y, Yagi T, Iwabuchi Y, et al. Combined analysis of pathoology and hemodynamics of human unruptured cerebral aneurysm with thin-walled region. In: Sunriver, Oregon, USA; 2013.
24. Tobe Y Pathological engineering for predicting transition of human cerebral aneurysms. In: Doctoral Dissertation. Waseda University, Japan; 2016:1–165.
25. Suzuki T, Takao H, Suzuki T, et al. Determining the Presence of Thin-Walled Regions at High-Pressure Areas in Unruptured Cerebral Aneurysms by Using Computational Fluid Dynamics. Neurosurgery 2016;79:589–95. [PubMed: 27028475]

26. Tobe Y, Yagi T, Iwabuchi Y, et al. Relationship between Pathology and Hemodynamics of Human Unruptured Cerebral Aneurysms. In: Goh J, ed. The 15th International Conference on Biomedical Engineering. Springer International Publishing; 2014:44–7.

27. Frösen J, Piippo A, Paetau A, et al. Remodeling of Saccular Cerebral Artery Aneurysm Wall Is Associated With Rupture: Histological Analysis of 24 Unruptured and 42 Ruptured Cases. Stroke 2004;35:2287–93. [PubMed: 15322297]

28. Omodaka S, Sugiyama S, Inoue T, et al. Local hemodynamics at the rupture point of cerebral aneurysms determined by computational fluid dynamics analysis. Cerebrovasc Dis 2012;34:121–9. [PubMed: 22965244]

29. Fukazawa K, Ishida F, Umeda Y, et al. Using Computational Fluid Dynamics Analysis to Characterize Local Hemodynamic Features of Middle Cerebral Artery Aneurysm Rupture Points. World Neurosurg 10.1016/j.wneu.2013.02.012.

30. Sugiyama S, Niizuma K, Nakayama T, et al. Relative residence time prolongation in intracranial aneurysms: a possible association with atherosclerosis. Neurosurgery 2013;73:767–76. [PubMed: 23863763]

31. Sugiyama S-I, Endo H, Niizuma K, et al. Computational Hemodynamic Analysis for the Diagnosis of Atherosclerotic Changes in Intracranial Aneurysms: A Proof-of-Concept Study Using 3 Cases Harboring Atherosclerotic and Nonatherosclerotic Aneurysms Simultaneously. Comput Math Methods Med 2016;2016:2386031. [PubMed: 27703491]

32. Talari S, Kato Y, Shang H, et al. Comparison of computational fluid dynamics findings with intraoperative microscopy findings in unruptured intracranial aneurysms- An initial analysis. Asian J Neurosurg 2016;11:356–60. [PubMed: 27695537]

33. Furukawa K, Ishida F, Tsuji M, et al. Hemodynamic characteristics of hyperplastic remodeling lesions in cerebral aneurysms. PloS One 2018;13:e0191287. [PubMed: 29338059]

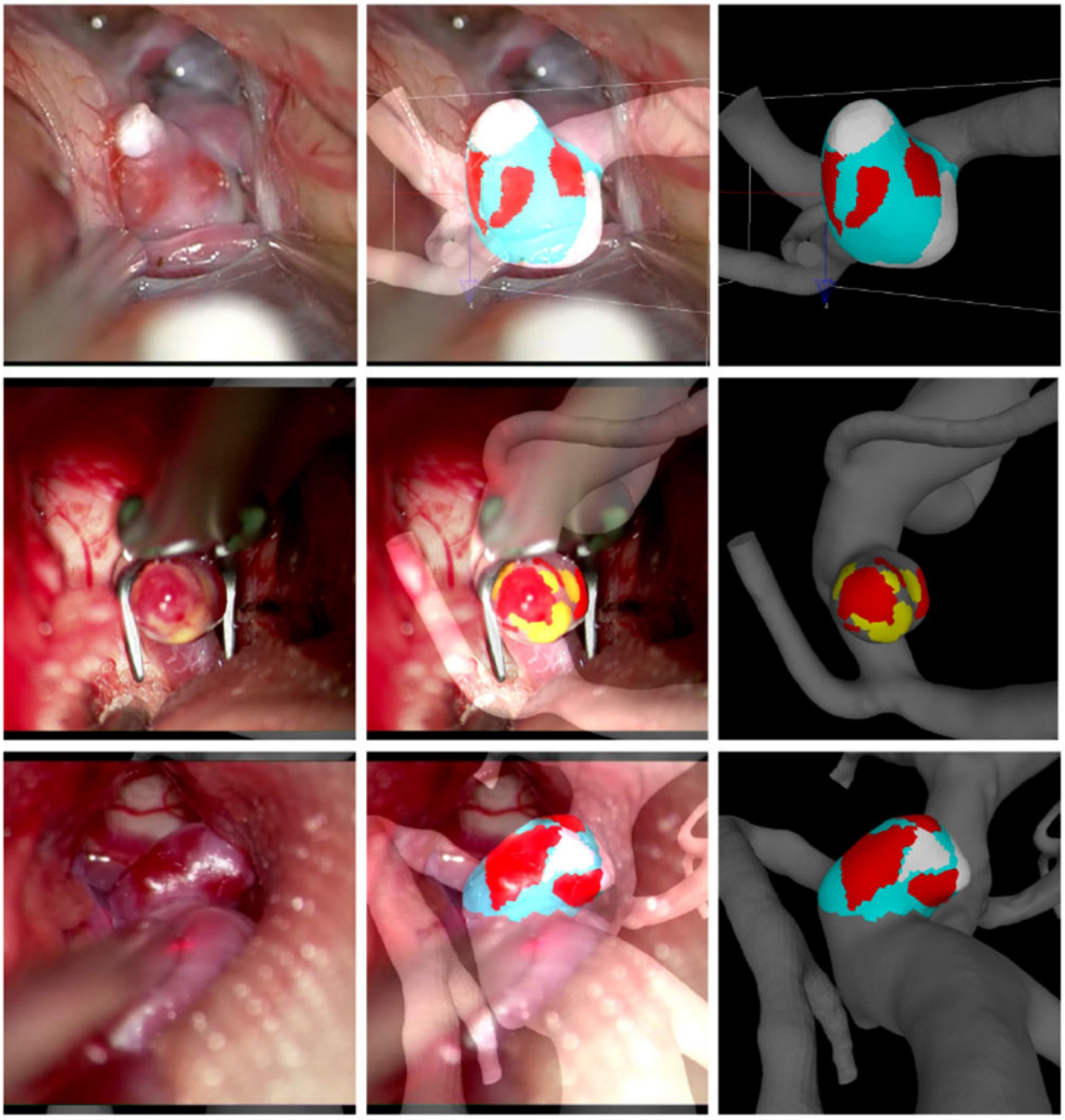

Figure 1.

Marking aneurysm regions in three example aneurysms. Left column: selected frames of intra-operative videos displaying aneurysm wall. Center column: superposition of semi-transparent video frame and marked 3D vascular model. Right column: final virtual marking of aneurysm wall regions (Red=thin, Yellow=atherosclerotic, White=Hyperplastic, Cyan=normal looking).

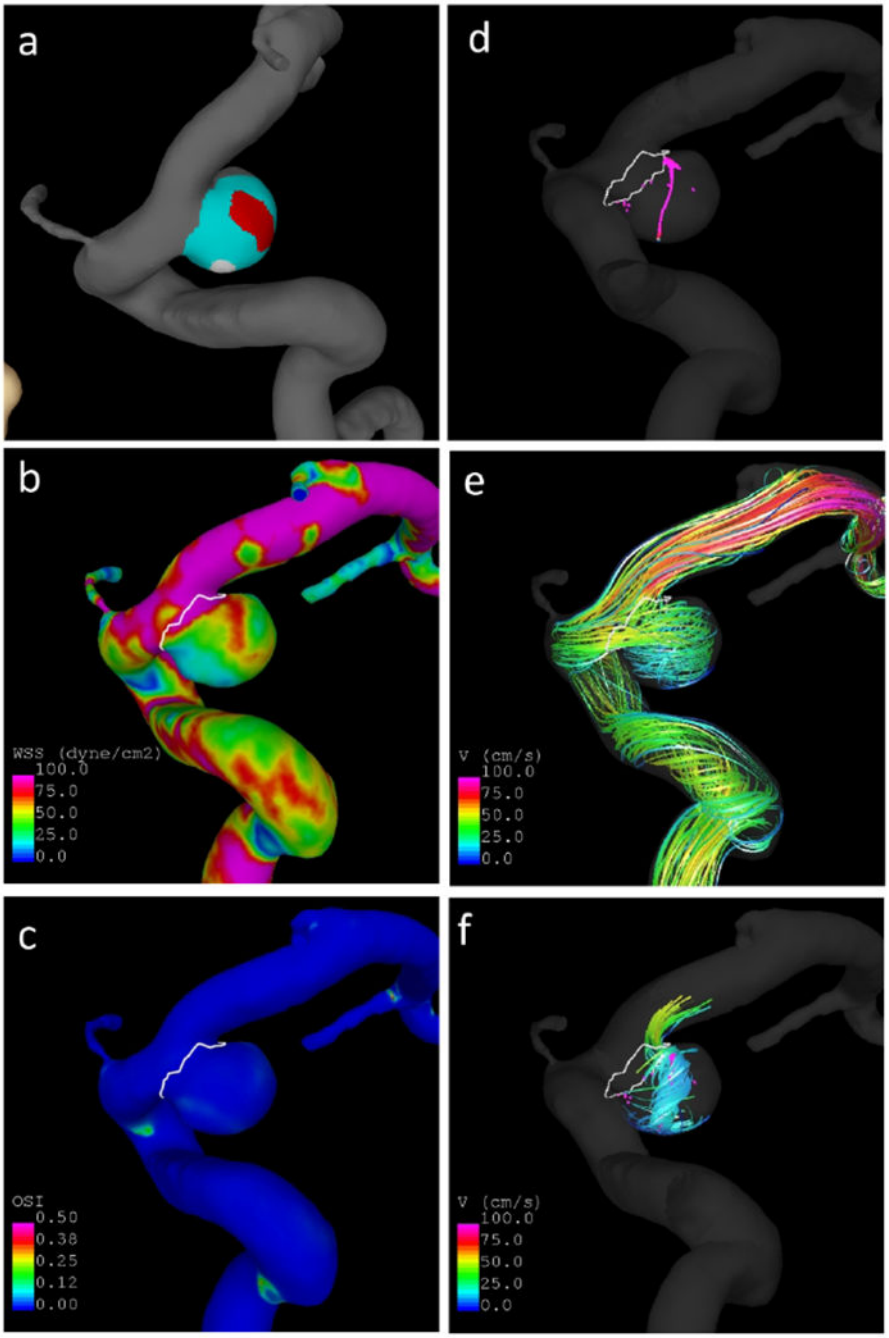

Figure 2.
Example aneurysm with thin and hyperplastic regions: a) wall regions (red=thin, white=hyperplastic, cyan=normal looking), b) wall shear stress, c) oscillatory shear index, d) vortex core-lines, e) flow streamlines, f) swirling around vortex core-lines.

Table 1:

P-values of pairwise comparisons of pathological and normal looking aneurysm regions. Significant values (adjusted for multiple regional tests) are indicated with a "*". Significant values after a further adjustment for testing multiple hemodynamic variables are indicated with a **. The region with the larger value is indicated in parenthesis next to the significant p-values. A=atherosclerotic, H=hyperplastic, T=thin, R=ruptured, N=normal looking.

Variable	A vs N	H vs N	T vs N	R vs N
OSImax	<0.001** (N)	<0.001** (N)	<0.001** (N)	<0.001** (N)
OSIavg	0.8	0.98	0.006** (N)	0.33
OSImin	<0.001** (A)	<0.001** (H)	<0.001** (T)	<0.001** (R)
WSSmax	<0.001** (N)	<0.001** (N)	<0.001** (N)	<0.001** (N)
WSSavg	0.01** (N)	0.005** (N)	0.54	0.005** (N)
WSSmin	0.01** (A)	<0.001** (H)	<0.001** (T)	0.1
PREmax	<0.001** (N)	<0.001** (N)	<0.001** (N)	0.05* (N)
PREavg	0.06	0.009** (N)	0.59	0.03* (R)
PREmin	<0.001** (A)	0.001** (H)	<0.001** (T)	<0.001** (R)
RRTmax	0.004** (N)	<0.001** (N)	<0.001** (N)	0.005** (N)
RRTavg	0.67	0.36	<0.001** (N)	0.47
RRTmin	<0.001** (A)	<0.001** (H)	<0.001** (T)	0.04* (R)
GONmax	<0.001** (N)	0.001** (N)	<0.001** (N)	<0.001** (N)
GONavg	0.54	0.85	<0.001** (N)	0.04* (N)
GONmin	<0.001** (A)	<0.001** (H)	<0.001** (T)	0.008** (R)
WSSDIVmax	0.06	0.03** (N)	<0.001** (N)	0.06
WSSDIVavg	0.93	0.79	0.93	0.93
WSSDIVmin	0.21	0.21	0.06	0.21
WSSGRDmax	<0.001** (N)	<0.001** (N)	<0.001** (N)	<0.001** (N)
WSSGRDavg	0.38	0.09	0.82	0.07
WSSGRDmin	0.007** (A)	0.007** (H)	<0.001** (T)	0.1

Table 2:

P-values of pairwise comparisons of pathological aneurysm regions. Significant values (adjusted for multiple regional tests) are indicated with a “*”. Significant values after a further adjustment for testing multiple hemodynamic variables are indicated with a **. The region with the larger value is indicated in parenthesis next to the significant p-values. A=atherosclerotic, H=hyperplastic, T=thin, R=ruptured, N=normal looking.

Variable	A vs H	A vs T	A vs R	H vs T	H vs R	T vs R
OSImax	0.77	0.03* (A)	0.35	0.002** (H)	0.32	0.45
OSIavg	0.66	0.05* (A)	0.33	0.04* (H)	0.33	0.86
OSImin	0.09	0.46	0.46	0.29	0.52	0.98
WSSmax	0.74	0.74	0.4	0.96	0.14	0.14
WSSavg	0.81	0.06	0.47	0.006** (T)	0.2	0.01* (T)
WSSmin	0.76	0.003* (T)	0.76	<0.001** (T)	0.66	0.01* (T)
PREmax	0.55	0.42	0.47	0.69	0.69	0.69
PREavg	0.5	0.1	0.01* (R)	0.009** (T)	0.009* (R)	0.09
PREmin	0.01* (A)	0.79	0.01* (R)	0.003** (T)	<0.001** (R)	0.01* (R)
RRTmax	0.98	0.007* (A)	0.5	<0.001** (H)	0.42	0.42
RRTavg	0.8	0.03* (A)	0.47	<0.001** (H)	0.36	0.67
RRTmin	0.82	0.82	0.82	0.82	0.82	0.82
GONmax	0.24	0.24	0.55	<0.001** (H)	0.12	0.7
GONavg	0.6	0.19	0.6	0.002** (H)	0.19	0.8
GONmin	0.49	0.66	0.57	0.85	0.92	0.75
WSSDIVmax	0.93	0.46	0.54	0.28	0.54	0.93
WSSDIVavg	0.8	0.93	0.93	0.93	0.93	0.96
WSSDIVmin	0.83	0.96	0.96	0.54	0.83	0.96
WSSGRDmax	0.75	0.89	0.31	0.75	0.08	0.08
WSSGRDavg	0.82	0.39	0.38	0.07	0.38	0.07
WSSGRDmin	0.6	0.02* (T)	0.64	<0.001** (T)	0.88	0.01* (T)